Heliyon 8 (2022) e09869

Contents lists available at ScienceDirect

Heliyon

journal homepage: www.cell.com/heliyon

Research article

A GC–MS-based untargeted metabolomics approach for comprehensive metabolic profiling of vancomycin-induced toxicity in mice

Changmeng Cui [a,1], Li Zhu [b,1], Qian Wang [c], Ruijuan Liu [d], Dadi Xie [e], Yujin Guo [b,**], Dingyi Yu [f], Changshui Wang [a], Dan Chen [b], Pei Jiang [b,*]

[a] Department of Neurosurgery, Affiliated Hospital of Jining Medical University, Jining 272000, China
[b] Institute of Clinical Pharmacy and Pharmacology, Jining First People's Hospital, Jining Medical University, Jining 272000, China
[c] Department of Clinical Medicine, Jining Medical University, Jining 272000, China
[d] Department of Pulmonary and Critical Care Medicine, Jining First People's Hospital, Jining 272000, China
[e] Tengzhou Central People's Hospital, Tengzhou 277500, China
[f] Jining Life Science Center, Jining 272000, China

ARTICLE INFO

Keywords:
Vancomycin
Biomarker
Gas chromatography-mass spectrometry
Metabolomics
Toxicity

ABSTRACT

Background: Vancomycin is a glycopeptide antibiotic that is commonly used for severe drug-resistant infections treatment. Application of vancomycin frequently leads to severe ototoxicity, hepatotoxicity, and nephrotoxicity; however, the comprehensive metabolic analysis of vancomycin-induced toxicity is lacking.
Purpose: This study attempted to investigate the metabolic changes after vancomycin administration in mice.
Methods: Experimental mice (n = 9) received continuous intraperitoneal injection of vancomycin (400 mg/kg) every day for 7 days, and mice in control group (n = 9) were treated with the same amount of normal saline. Pathological changes of the kidney were examined using haematoxylin and eosin (HE) staining. A gas chromatography-mass spectrometry (GC-MS) approach was used to identify discriminant metabolites in serum and various organs including the heart, liver, kidney, spleen, cerebral cortex, hippocampus, inner ear, lung, and intestine. The potential metabolites were identified using orthogonal partial least squares discrimination analysis (OPLS-DA). Subsequently, the MetaboAnalyst 5.0 (http://www.metaboanalyst.ca) and Kyoto Encyclopedia of Genes and Genomes database (KEGG, http://www.kegg.jp) were employed to depict the metabolic pathways.
Results: Compared with the control group, the vancomycin induced 13, 17, 27, 22, 16, 10, 17, 11, 10, and 7 differential metabolites in the serum, liver, kidney, heart, cerebral cortex, lung, spleen, intestine, hippocampus, and inner ear, respectively. Further pathway analyses identified that amino acids metabolism, fatty acids biosynthesis, energy metabolism, and lipid metabolism were disrupted after VCM exposure.
Conclusion: Vancomycin affects the metabolism in various organs in mice, which provides new insights for identification of vancomycin-induced toxicity, and facilitate to better understanding of the metabolic pathogenesis of vancomycin.

1. Introduction

Vancomycin (VCM) is frequently used for treating pseudomembranous colitis, staphylococcal enterocolitis, bacterial endocarditis, and septicemia [1]. Besides, VCM is one of the first-line treatments for severely drug-resistant gram-positive infections, such as methicillin-resistant *staphylococcus aureus* (MRSA), methicillin-resistant coagulase-negative *Staphylococcus*, and other gram-positive-induced severe drug-resistant infections [2]. Unfortunately, VCM-induced adverse effects are frequently reported, mainly including hypotension, phlebitis, nephrotoxicity, ototoxicity, red man syndrome, neutropenia, chills, and fever [3, 4]. Moreover, compelling evidence suggests that oral VCM results in gut dysbiosis [5].

Studies have shown that VCM treatment alters the metabolism of uracil, amino acids, and short-chain fatty acids, indicating that antibiotics such as VCM can disrupt metabolic profiling and harm health [1, 2].

* Corresponding author.
** Corresponding author.
E-mail addresses: guoyujin99@126.com (Y. Guo), jiangpeicsu@sina.com (P. Jiang).
[1] These authors contributed equally to this work.

https://doi.org/10.1016/j.heliyon.2022.e09869
Received 30 March 2022; Received in revised form 16 May 2022; Accepted 30 June 2022

In patients with metabolic syndrome, oral vancomycin intake apparently not only affects intestinal microbiota diversity, but also changes bile acid metabolism and insulin sensitivity [6]. Recently, it has been reported that a variety of lysophospholipids metabolisms are involved in VCM stimuli-caused nephrotoxicity [7]. However, there is a lack of comprehensive investigation of metabolic profiling after VCM exposure.

Metabolomics is an important approach used in systems biology research and its main purpose is to systematically identify potential metabolic biomarkers when some stimulation or impact happened. As the end products and intermediates of cellular regulatory processes, metabolites reflect the phenotypical variations in live organisms, and therefore, metabolomics can be employed in agriculture, human disease, and pharmacology research [8, 9, 10]. A variety of biological samples can be used in metabolomics studies, including the urine, serum, saliva, and liver and heart. Moreover, there are various analytical methods, including nuclear magnetic resonance spectroscopy, ultra-high-performance liquid chromatography combined with quadrupole time-of-flight mass spectrometry, and GC-MS [11, 12]. When combined with multivariate statistical analysis, these analytical approaches facilitate the screening and identification of potential metabolites [13, 14]. An untargeted GC-MS coupled with targeted lipidomic analysis has been applied to investigate the metabolic changes and lipid metabolism in VCM-treated kidney cells, and the results unveiled that several lipids including glycosphingolipids and phosphatidylethanolamines were increased in mIMCD-3 cells, and both mIMCD-3 cells and MDCK cells promoted anabolic glucose reactions, leading to elevated sorbitol and lactate expression [15]. Additionally, a GC-TOFMS-based untargeted metabolic approach has indicated that oral vancomycin leads to gut bacterial microbiota changes and metabolic variations [16]. However, to date, most studies on VCM-induced biotoxicity have been conducted in single organs, and the corresponding changes in metabolic profiling in different tissues have not been studied.

Therefore, a GC-MS-based untargeted metabolomics approach was employed to investigate the metabolic alterations after VCM exposure in this study. Changes in metabolites of various organs and tissues as well as disrupted metabolic pathways were evaluated to elucidate the metabolic profiling after VCM exposure. This study represents the first comprehensive investigation of metabolic alterations in VCM-treated mice.

2. Materials and methods

2.1. Chemicals and reagents

Vancomycin (USP ≥950 μg/mg), heptadecanoic acid (purity ≥98%), methanol (chromatographic grade) and pyridine were obtained from Shanghai Macklin Biochemical (Shanghai, China). O-methylhydroxylamine hydrochloride (purity ≥98%) was purchased from J&K Scientific Ltd. (Beijing, China). N, O-bis(trimethylsilyl)trifluoroacetamide (containing 1% trimethylchlorosilane) was obtained from Sigma Aldrich (St. Louis, MO. USA). The purified water was purchased from Hangzhou Wahaha Company (Hangzhou, China).

2.2. Animal treatment

A total of 18 male outbred Kunming mice (6 weeks) were obtained from Jinan Pengyue Experimental Animal Breeding Co., Ltd. (Jinan, China), and kept at 22 ± 2 °C with 60–70% humidity under a 12 h/12 h day/night cycle. All mice were fed standard rodent food and water *ad libitum*. After 1 week of acclimatization prior to experiment, mice were randomly divided into the control and VCM groups. Mice in VCM group (n = 9) were intraperitoneally injected with VCM (400 mg/kg) every day for 7 days. Nine mice treated with the same amount of normal saline served as a control group (n = 9). This study was approved by the Ethical Committee for Animal Experimentation of Jining Medical University (Approval No. JNMC-2022-DW-041).

2.3. Sample collection

Mice were anesthetized by intraperitoneal injection of 10% chloral hydrate. Blood samples (approximately 1 mL each mouse) were collected into 1.5-mL Eppendorf tubes after eyeball enucleation. After centrifugation at 4000 rpm for 10 min at 4 °C, serum samples were obtained and stored at -80 °C until analysis. Animals were sacrificed by cervical dislocation. Immediately thereafter, the liver, kidney, heart, cerebral cortex, lung, spleen, intestine, hippocampus, and inner ear tissues were collected on ice, washed with phosphate-buffered saline (pH 7.2), frozen in liquid nitrogen immediately, and stored at -80 °C.

2.4. Pathological examination

The kidney tissues were obtained, fixed with 4 % paraformaldehyde overnight, and embedded in paraffin after washing with 70 % ethanol (1 h) and 95 % ethanol (1 h). Subsequently, 4 μm thick sections were prepared, deparaffinated and rehydrated with xylene (5 min, thrice), 100 % ethanol (2 min, twice), 96 % ethanol (2 min), 80 % ethanol (2 min), 70 % ethanol (2 min), and 50 % ethanol (2 min). Sections were stained with HE (Sigma, USA). A Whole Slide Imaging Pannoramic SCAN (PANNORAMIC DESK/MIDI/250/1000, 3DHISTECH, Hungary), and a scanning and browsing software (CaseViewer 2.4, 3DHISTECH, Hungary) were employed for histopathology examination.

2.5. Sample preparation

A total of 100 μL of serum was mixed with 350 μL of heptadecanoic acid (100 μg/mL in methanol), and the mixture was vortexed and centrifuged at 14,000 rpm for 15 min at 4 °C. Afterwards, the supernatant was transferred into a 1.5-mL Eppendorf tube and dried under nitrogen gas at 37 °C. The extracts were subsequently mixed with 80 μL of O-methylhydroxylamine hydrochloride (15 mg/mL in pyridine) and incubated at 70 °C for 90 min. Next, 100 μL of N, O-bis(trimethylsilyl)trifluoroacetamide (containing 1 % trimethylchlorosilane) was added, followed by incubation at 70 °C for 1 h. After vortexing, the solution was centrifuged at 4 °C for 2 min at 3000 rpm. A 0.22-μm pore membrane filter was used for sample filtering before GC-MS analysis.

For tissue sample preparation, a total of 50 mg of each tissue sample was homogenized with 1 mL of methanol in a grinding tube. 50 μL of heptadecanoic acid (1 mg/ml in methanol) was added into tissue homogenates, and centrifuged at 4 °C for 15 min at 14,000 rpm. Then, 80 μL of O-methylhydroxylamine hydrochloride (15 mg/mL in pyridine) was added. After incubation at 70 °C for 90 min, samples were mixed with 100 μL of N, O-bis(trimethylsilyl)trifluoroacetamide (containing 1% trimethylchlorosilane) at 70 °C for 60 min. A 0.22-μm filter was applied for sample purification. Pooling 10 μL of each sample of control group and VCM group as quality control (QC).

2.6. GC-MS analyses

Biofluids were analyzed by GC-MS using a 7000C mass spectrometer with a 7890 B GC system (Agilent Technologies, USA) equipped with an HP-5MS fused silica capillary column. Helium was used as the carrier gas, and the flow rate was set to 1 mL/min. An aliquot of 1 μL sample was injected into GC-MS with a split ratio of 50:1. The injection temperature was set to 280 °C, transfer line temperature was 250 °C, and ion source temperature was 230 °C, respectively. Electron collision ionization was -70 EV, and the frequency of acquisition was 20 spectra/s. MS was performed via electrospray ionization with a mass/charge (m/z) full scan range of 50–800.

2.7. Data processing and metabolite identification

Data obtained from GC-MS were analyzed using the Agilent Mass Hunter (Version B.07.00, Agilent Technologies, CA, USA). The raw data

were converted to the m/z data format. The metabolites in this study could be categorized as Level 2 – Putatively annotated compounds (i.e., identification was based only in the mass spectrum similarity with commercial spectral libraries, retention indexes and reverse percentage of match) [17]. Briefly, we created a library containing all QC samples, and the U.S. National Institute of Standards and Technology (NIST 14) GC-MS library was used to identify the unknown metabolites from QC, followed by alignment, retention time correction, baseline filtration, and deconvolution. The metabolites with similarity >80% were considered as structurally identified. All metabolite identifications were manually validated to reduce deconvolution errors during automated data-processing and to eliminate false identifications. Afterwards, a new spectrum library named

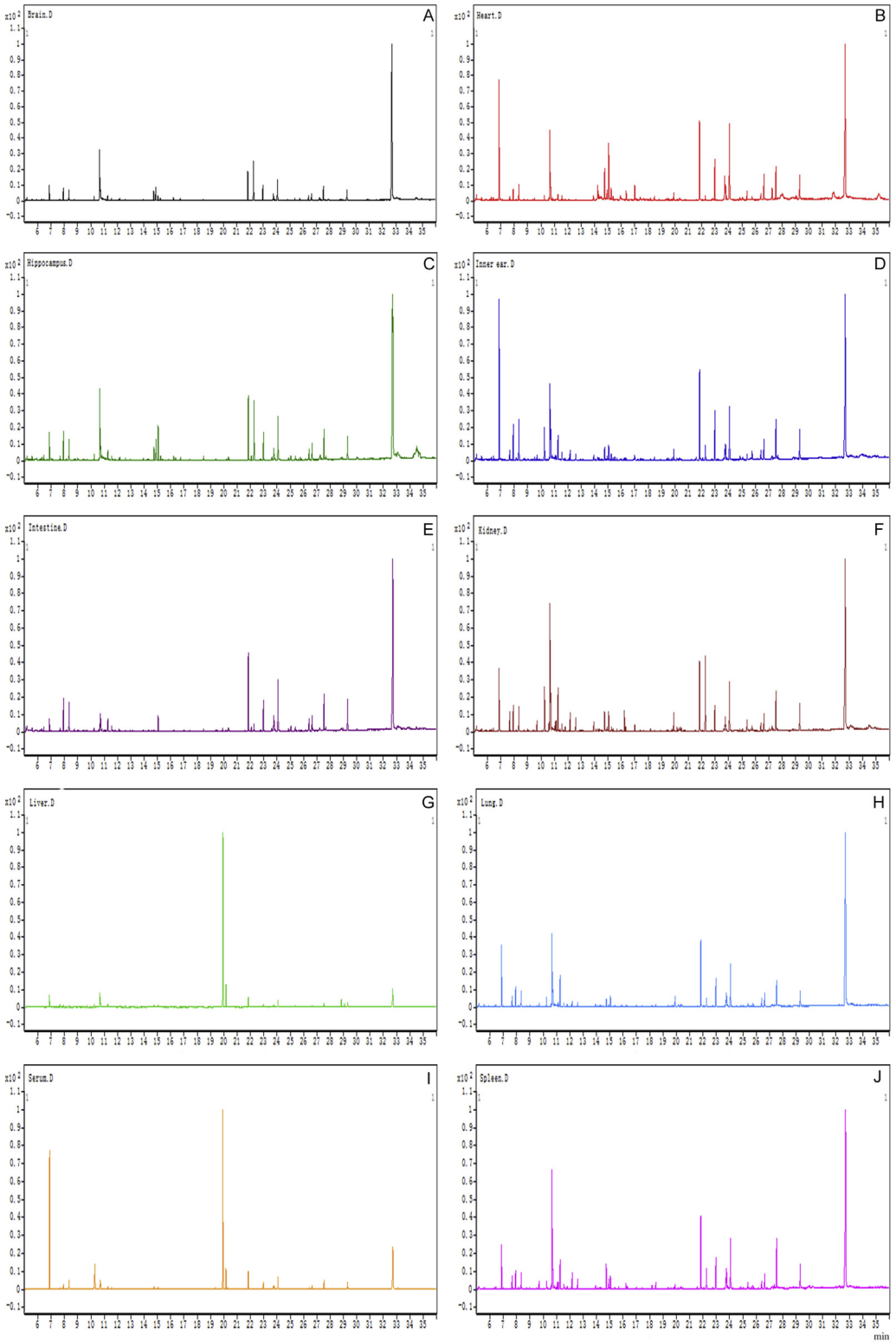

Figure 1. Representative gas chromatography–mass spectrometry (GC–MS) total ion chromatograms (TICs) of quality control (QC). (A) Cerebral cortex (B) Heart (C) Hippopotamus (D) Inner ear (E) Intestine (F) Kidney (G) Liver (H) Lung (I) Serum (J) Spleen.

Table 1. The scores of the model parameters.

Tissue	R^2X (cum)	R^2Y (cum)	Q^2 (cum)
Serum	0.43	0.998	0.802
Liver	0.466	0.905	0.766
Kidney	0.815	0.893	0.739
Hippocampus	0.834	0.941	0.836
Heart	0.425	0.993	0.831
Inner ear	0.698	0.995	0.758
Spleen	0.628	0.999	0.675
Lung	0.518	0.951	0.728
Intestine	0.646	0.993	0.873
Cerebral cortex	0.565	0.955	0.934

"New Library" was obtained, which was employed for spectrum matching of metabolites in experimental samples. Finally, an integrated data matrix composed of the peak index (RT-m/z pair), sample name, and corresponding peak area was generated.

Subsequently, the peak area from the data matrix was normalized using Microsoft Excel™ (Microsoft, Redmond, WA, USA). The processed data were analyzed using a set of multivariate statistical methods initially composed of principal components analysis and OPLS-DA using SIMCA-P 14.0 (Umetrics, Sartorius Stedim Biotech). Permutation testing was conducted to evaluate the robustness of the OPLS-DA models. The comparison between the two groups was conducted using two-tailed Student's *t*-tests.

2.8. Metabolic pathway analysis

Compounds with variable importance in projection (VIP) values >1.0 and two-tailed Student's *t*-test p values <0.05 were considered as potential discriminant metabolites. Pathway analysis was performed using MetaboAnalyst 5.0 (http://www.metaboanalyst.ca) and KEGG database (http://www.kegg.jp). Pathways with raw *p* values <0.05 and impact values >0 were considered as statistically significant.

3. Results

3.1. GC-MS TICs

Representative GC-MS total ion chromatograms (TICs) of QC from serum and tissue samples are presented in Figure 1. Differences in TICs among different QC samples could be observed.

3.2. Multivariate analysis of metabolomic data

The scores of the model parameters of OPLS-DA were detailed in Table 1, and the values of each parameter were close to 1.0. A ranking

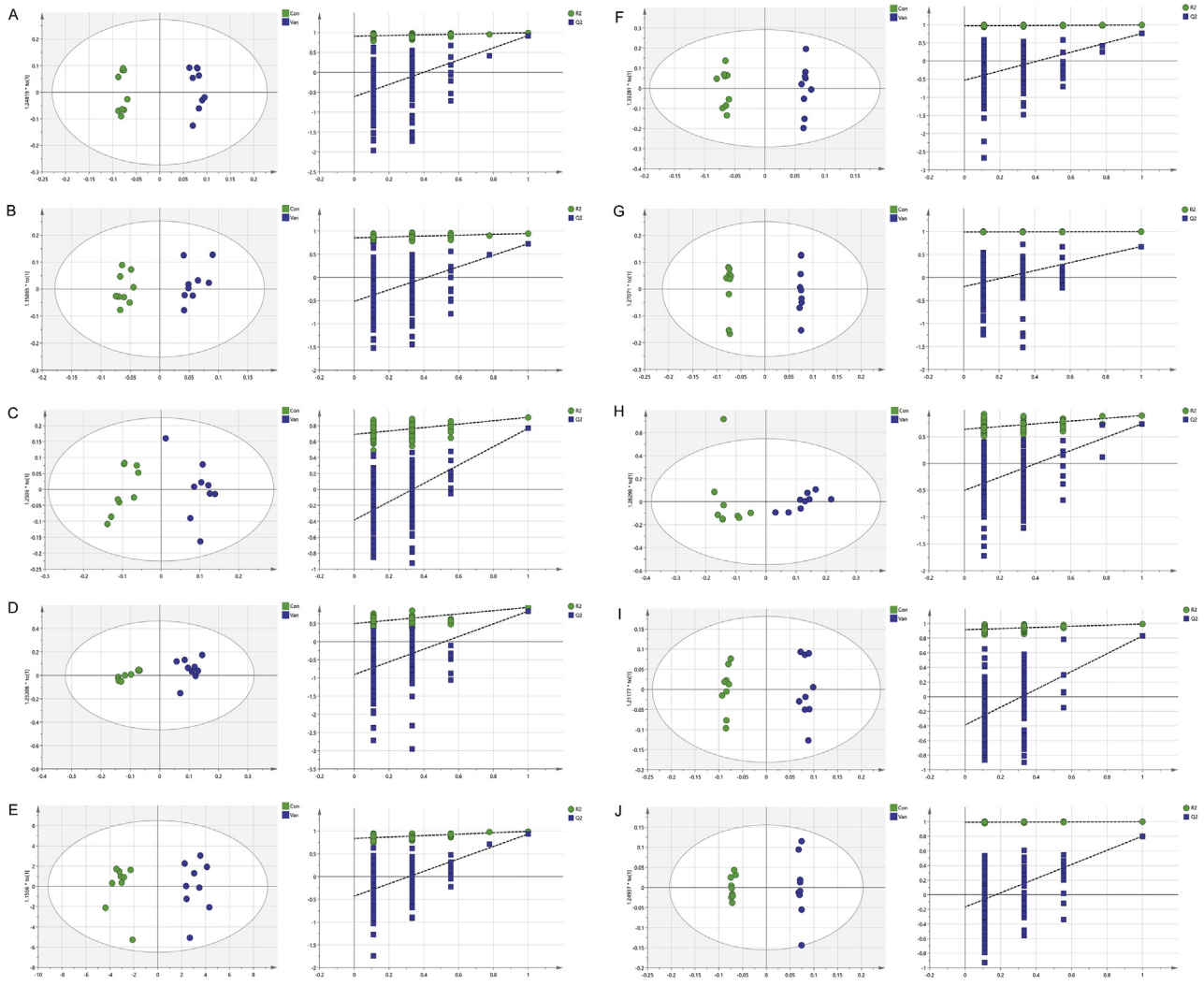

Figure 2. OPLS-DA score plots and 200 permutation tests. (A) Intestine (B) Lung (C) Liver (D) Hippocampus (E) Cerebral cortex (F) Inner ear (G) Spleen (H) Kidney (I) Heart (J) Serum.

Table 2. Differential metabolites in different tissues and serum samples after VCM treatment.

Samples	Metabolites	HMDB ID	VIP	*p*-value	Fold change	Trend
Serum	4-Hydroxyproline	HMDB0000725	1.481	<0.05	0.50	↓
	Glycine	HMDB0000123	2.261	<0.05	6.38	↑
	L-Alanine	HMDB0000161	2.634	<0.05	17.02	↑
	L-Isoleucine	HMDB0000172	2.485	<0.05	5.13	↑
	L-Phenylalanine	HMDB0000159	1.937	<0.05	4.29	↑
	L-Proline	HMDB0000162	2.304	<0.05	3.70	↑
	L-Threonine	HMDB0000167	2.355	<0.05	4.52	↑
	L-Valine	HMDB0000883	2.814	<0.05	0.57	↓
	Malic acid	HMDB0000744	1.768	<0.05	0.45	↓
	Myo-Inositol	HMDB0000211	1.421	<0.05	1.69	↑
	Serine	HMDB0062263	2.727	<0.05	9.25	↑
	Uracil	HMDB0000300	1.325	<0.05	1.91	↑
	Urea	HMDB0000294	2.323	<0.05	3.85	↑
Liver	Docosahexaenoic acid	HMDB0002183	1.061	<0.05	0.55	↓
	D-Ribose	HMDB0000283	1.127	<0.05	0.49	↓
	Gamma-Aminobutyric acid	HMDB0000112	1.697	<0.05	6.38	↑
	Glycine	HMDB0000123	1.701	<0.05	4.57	↑
	L-Alanine	HMDB0000161	1.356	<0.05	4.47	↑
	L-Aspartic acid	HMDB0000191	1.847	<0.05	9.60	↑
	L-Cysteine	HMDB0000574	1.524	<0.05	3.38	↑
	L-Glutamic acid	HMDB0000148	1.951	<0.05	8.78	↑
	L-Isoleucine	HMDB0000172	2.034	<0.05	12.30	↑
	L-Leucine	HMDB0000687	2.008	<0.05	10.23	↑
	L-Proline	HMDB0000162	2.026	<0.05	16.65	↑
	L-Threonine	HMDB0000167	1.763	<0.05	10.21	↑
	L-Tyrosine	HMDB0000158	1.924	<0.05	14.34	↑
	Palmitelaidic acid	HMDB0012328	1.089	<0.05	1.92	↑
	L-Valine	HMDB0000883	2.006	<0.05	11.12	↑
	Uracil	HMDB0000300	1.341	<0.05	2.96	↑
	Urea	HMDB0000294	1.721	<0.05	4.62	↑
Kidney	Hexadecane	HMDB0033792	1.059	<0.05	0.11	↓
	4-Hydroxyproline	HMDB0000725	1.19	<0.05	5.56	↑
	Docosahexaenoic acid	HMDB0002183	1.154	<0.05	3.06	↑
	Gamma-Aminobutyric acid	HMDB0000112	1.360	<0.05	6.01	↑
	Inosine	HMDB0000195	1.222	<0.05	0.11	↓
	L-Alanine	HMDB0000161	1.248	<0.05	25.66	↑
	L-Asparagine	HMDB0000168	1.391	<0.05	0.04	↓
	L-Aspartic acid	HMDB0000191	1.322	<0.05	45.83	↑
	L-Glutamic acid	HMDB0000148	1.27	<0.05	15.39	↑
	L-Isoleucine	HMDB0000172	1.374	<0.05	29.91	↑
	L-Lactic acid	HMDB0000190	1.122	<0.05	0.22	↓
	L-Methionine	HMDB0000696	1.337	<0.05	30.40	↑
	L-Phenylalanine	HMDB0000159	1.482	<0.05	38.45	↑
	L-Proline	HMDB0000162	1.309	<0.05	49.11	↑
	L-Threonine	HMDB0000167	1.628	<0.05	57.36	↑
	L-Tyrosine	HMDB0000158	1.310	<0.05	4.48	↑
	MG (0:0/18:0/0:0)	HMDB0011535	1.114	<0.05	0.14	↓
	Niacinamide	HMDB0001406	1.333	<0.05	6.95	↑
	Octadecane	HMDB0033721	1.01	<0.05	0.19	↓
	O-Phosphoethanolamine	HMDB0000224	1.106	<0.05	4.00	↑
	Pyroglutamic acid	HMDB0000267	1.511	<0.05	25.82	↑
	Amphetamine	HMDB0014328	1.342	<0.05	9.37	↑
	Ribitol	HMDB0000508	1.229	<0.05	0.19	↓
	Scyllo-Inositol	HMDB0006088	1.038	<0.05	0.21	↓
	Serine	HMDB0062263	1.616	<0.05	130.66	↑
	Sorbitol	HMDB0000247	1.084	<0.05	0.16	↓
	Uracil	HMDB0000300	1.396	<0.05	11.62	↑

(*continued on next page*)

Table 2 (*continued*)

Samples	Metabolites	HMDB ID	VIP	*p*-value	Fold change	Trend
Heart	Isopropyl alcohol	HMDB0000863	1.246	<0.05	0.57	↓
	3-Hydroxypicolinic acid	HMDB0013188	1.050	<0.05	1.56	↑
	4-Hydroxyproline	HMDB0000725	1.380	<0.05	2.23	↑
	Arachidonic acid	HMDB0001043	1.559	<0.05	2.30	↑
	Docosahexaenoic acid	HMDB0002183	1.408	<0.05	4.31	↑
	Ethanolamine	HMDB0000149	1.403	<0.05	2.06	↑
	Glyceric acid	HMDB0000139	1.681	<0.05	2.66	↑
	Glycerol	HMDB0000131	1.167	<0.05	1.53	↑
	Glycine	HMDB0000123	1.33	<0.05	1.95	↑
	L-Alanine	HMDB0000161	1.893	<0.05	3.53	↑
	L-Aspartic acid	HMDB0000191	1.578	<0.05	2.35	↑
	L-Isoleucine	HMDB0000172	2.553	<0.05	17.90	↑
	L-Lactic acid	HMDB0000190	1.161	<0.05	1.65	↑
	L-Proline	HMDB0000162	2.419	<0.05	10.87	↑
	L-Threonine	HMDB0000167	2.355	<0.05	9.11	↑
	L-Valine	HMDB0000883	2.406	<0.05	8.96	↑
	Malic acid	HMDB0000744	1.135	<0.05	1.94	↑
	Oleic acid	HMDB0000207	1.362	<0.05	1.96	↑
	O-Phosphoethanolamine	HMDB0000224	1.737	<0.05	2.63	↑
	Pyroglutamic acid	HMDB0000267	1.627	<0.05	2.58	↑
	Serine	HMDB0062263	2.562	<0.05	36.46	↑
	Uracil	HMDB0000300	1.922	<0.05	0.99	↓
Cerebral cortex	Citric acid	HMDB0000094	1.362	<0.05	4.75	↑
	Docosahexaenoic acid	HMDB0002183	1.090	<0.05	2.33	↑
	Ethanolamine	HMDB0000149	1.109	<0.05	3.60	↑
	Gamma-Aminobutyric acid	HMDB0000112	1.152	<0.05	5.14	↑
	L-Aspartic acid	HMDB0000191	1.117	<0.05	3.96	↑
	L-Cysteine	HMDB0000574	1.358	<0.05	9.18	↑
	L-Glutamic acid	HMDB0000148	1.865	<0.05	31.64	↑
	L-Homoserine	HMDB0000719	1.709	<0.05	12.87	↑
	L-Phenylalanine	HMDB0000159	1.177	<0.05	3.78	↑
	2-Pyrrolidinone	HMDB0002039	1.324	<0.05	5.20	↑
	p-Cymene	HMDB0005805	1.656	<0.05	7.77	↑
	L-Threonine	HMDB0000167	1.044	<0.05	4.19	↑
	MG (0:0/18:0/0:0)	HMDB0011535	1.065	<0.05	0.54	↓
	MG (16:0/0:0/0:0)	HMDB0011564	1.245	<0.05	0.40	↓
	Oleic acid	HMDB0000207	1.097	<0.05	1.96	↑
	O-Phosphoethanolamine	HMDB0000224	1.312	<0.05	5.91	↑
Lung	Citrulline	HMDB0000904	1.948	<0.05	2.36	↑
	L-Cysteine	HMDB0000574	1.496	<0.05	1.73	↑
	L-Valine	HMDB0000883	2.332	<0.05	2.80	↑
	Myristic acid	HMDB0000806	1.563	<0.05	0.61	↓
	Succinic acid	HMDB0000254	1.755	<0.05	1.94	↑
	Uracil	HMDB0000300	1.563	<0.05	1.74	↑
	Urea	HMDB0000294	2.942	<0.05	7.29	↑
	Vaccenic acid	HMDB0003231	1.941	<0.05	2.10	↑
	D-Mannose	HMDB0000169	1.496	<0.05	1.96	↑
	Pipecolic acid	HMDB0000070	1.516	<0.05	1.65	↑
Spleen	Arachidonic acid	HMDB0001043	1.235	<0.05	1.98	↑
	Cholesterol	HMDB0000067	1.086	<0.05	1.46	↑
	Gamma-Aminobutyric acid	HMDB0000112	1.064	<0.05	2.24	↑
	L-Aspartic acid	HMDB0000191	1.713	<0.05	3.94	↑
	L-Lysine	HMDB0000182	2.036	<0.05	8.92	↑
	L-Methionine	HMDB0000696	1.849	<0.05	3.70	↑
	L-Phenylalanine	HMDB0000159	1.682	<0.05	3.15	↑
	L-Threonine	HMDB0000167	1.464	<0.05	2.51	↑
	Formamide	HMDB0001536	1.727	<0.05	2.76	↑
	3-Methyl-2-oxovaleric acid	HMDB0000491	1.180	<0.05	1.58	↑
	L-Tyrosine	HMDB0000158	2.279	<0.05	13.94	↑
	MG (0:0/18:0/0:0)	HMDB0011535	1.097	<0.05	1.56	↑

(*continued on next page*)

Table 2 (*continued*)

Samples	Metabolites	HMDB ID	VIP	*p*-value	Fold change	Trend
	MG (16:0/0:0/0:0)	HMDB0011564	1.174	<0.05	1.68	↑
	Myo-Inositol	HMDB0000211	1.637	<0.05	2.68	↑
	Myristic acid	HMDB0000806	1.106	<0.05	0.65	↓
	Pyroglutamic acid	HMDB0000267	1.390	<0.05	1.97	↑
	Stearic acid	HMDB0000827	1.122	<0.05	1.51	↑
Intestine	L-Lactic acid	HMDB0000190	1.152	<0.05	1.45	↑
	Myristic acid	HMDB0000806	1.169	<0.05	0.57	↓
	MG (0:0/18:0/0:0)	HMDB0011535	1.528	<0.05	2.14	↑
	N-Dodecane	HMDB0031444	1.340	<0.05	2.09	↑
	Palmitic acid	HMDB0000220	1.293	<0.05	0.70	↓
	Scyllo-Inositol	HMDB0006088	1.784	<0.05	1.78	↑
	Undecane	HMDB0031445	1.194	<0.05	1.88	↑
	N-Decane	HMDB0031450	1.418	<0.05	2.11	↑
	Nonane	HMDB0029595	1.073	<0.05	1.61	↑
	Tetradecane	HMDB0059907	1.01	<0.05	1.17	↑
	Tridecanol	HMDB0013316	1.279	<0.05	1.84	↑
Hippocampus	Creatinine	HMDB0000562	1.016	<0.05	3.21	↑
	Docosahexaenoic acid	HMDB0002183	1.153	<0.05	4.96	↑
	L-Alanine	HMDB0000161	1.514	<0.05	7.80	↑
	L-Phenylalanine	HMDB0000159	1.590	<0.05	17.36	↑
	L-Proline	HMDB0000162	1.408	<0.05	6.38	↑
	MG (16:0/0:0/0:0)	HMDB0011564	1.302	<0.05	0.37	↓
	MG (0:0/18:0/0:0)	HMDB0011535	1.215	<0.05	0.43	↓
	N-Dodecane	HMDB0031444	1.022	<0.05	0.54	↓
	Serine	HMDB0062263	1.498	<0.05	63.38	↑
	2-Aminobenzoic acid	HMDB0001123	1.315	<0.05	5.09	↑
Inner ear	Arachidonic acid	HMDB0001043	2.168	<0.05	2.17	↑
	Docosahexaenoic acid	HMDB0002183	1.548	<0.05	2.10	↑
	Gamma-Butyrolactone	HMDB0000549	2.813	<0.05	13.52	↑
	Myo-Inositol	HMDB0000211	1.817	<0.05	2.66	↑
	Ribitol	HMDB0000508	1.382	<0.05	1.79	↑
	Undecane	HMDB0031445	1.124	<0.05	0.61	↓
	Urea	HMDB0000294	2.329	<0.05	4.44	↑

HMDB, Human Metabolome Database. VIP, variable influence on projection. Fold change, the VCM group/the control group.

test was used to verify the validity of OPLS-DA model, and the intersection points of the blue regression line (Q^2-point) and the vertical axis (left) are all negative (Figure 2), which indicated the model was reliable. The OPLS-DA showed an apparent difference between the VCM group and control group.

3.3. Identification of metabolic changes

The VIP and *p* values are the standard criteria for potential metabolites. Metabolites with VIP >1 from OPLS-DA and *p* value <0.05 from Student's *t*-test were considered significant metabolic perturbations between the two groups. In addition, fold-change > 1 indicated that the metabolite has an upward trend, while fold-change < 1 indicated a downward trend. The perturbed metabolites in tissues and serum between the two groups are summarized in Table 2. Finally, 10 increased metabolites and 3 decreased metabolites were found in serum after VCM challenge versus control group. In the liver, VCM exposure led to 17 altered metabolites including 15 up-regulated and 2 down-regulated metabolites. In the kidney, 27 differential products including 18 up-regulated and 9 down-regulated metabolites were identified. There were 22 differential metabolites (20 up-regulated and 2 down-regulated) in the heart. In addition, 16 metabolites (14 up-regulated and 2 down-regulated) in cerebral cortex, 10 metabolites (9 up-regulated and 1 down-regulated) in the lung, 17 metabolites (16 up-regulated and 1 down-regulated) in the spleen, 11 metabolites (9 up-regulated and 2 down-regulated) in the intestine, 10 metabolites (7 up-regulated and 3 down-regulated) in the hippocampus were observed. In the inner ear, changes in undecane, 4-hydroxybutanoic acid, urea, myo-inositol, arachidonic acid, doconexent, and urea were observed in VCM group.

Subsequently, the results of cluster analyses of differential metabolites between the two groups are displayed in Figure 3, which portrays an apparent difference between the two groups.

3.4. Analyses of metabolic pathways

Furthermore, Metaboanalyst 5.0 (http://www.metaboanalyst.ca) and KEGG database (http://www.kegg.jp) were employed to determine metabolic pathways after VCM treatment. Metabolic pathways with Raw P < 0.5 and Impact >0 were considered as potential disturbed pathways (Table 3 and Figure 4). A detailed metabolic network was shown in Figure 5. The results showed that VCM exposure affected various amino acid metabolic pathways, glutathione metabolism, butanoate metabolism, glyoxylate and dicarboxylate metabolism, nicotinate and nicotinamide metabolism, fatty acid biosynthesis, glycerolipid metabolism, and glycerophospholipid metabolism pathways.

3.5. Pathological examination

Vancomycin-induced nephrotoxicity is a common adverse reaction. In this study, pathological changes of kidney tissue induced by VCM were

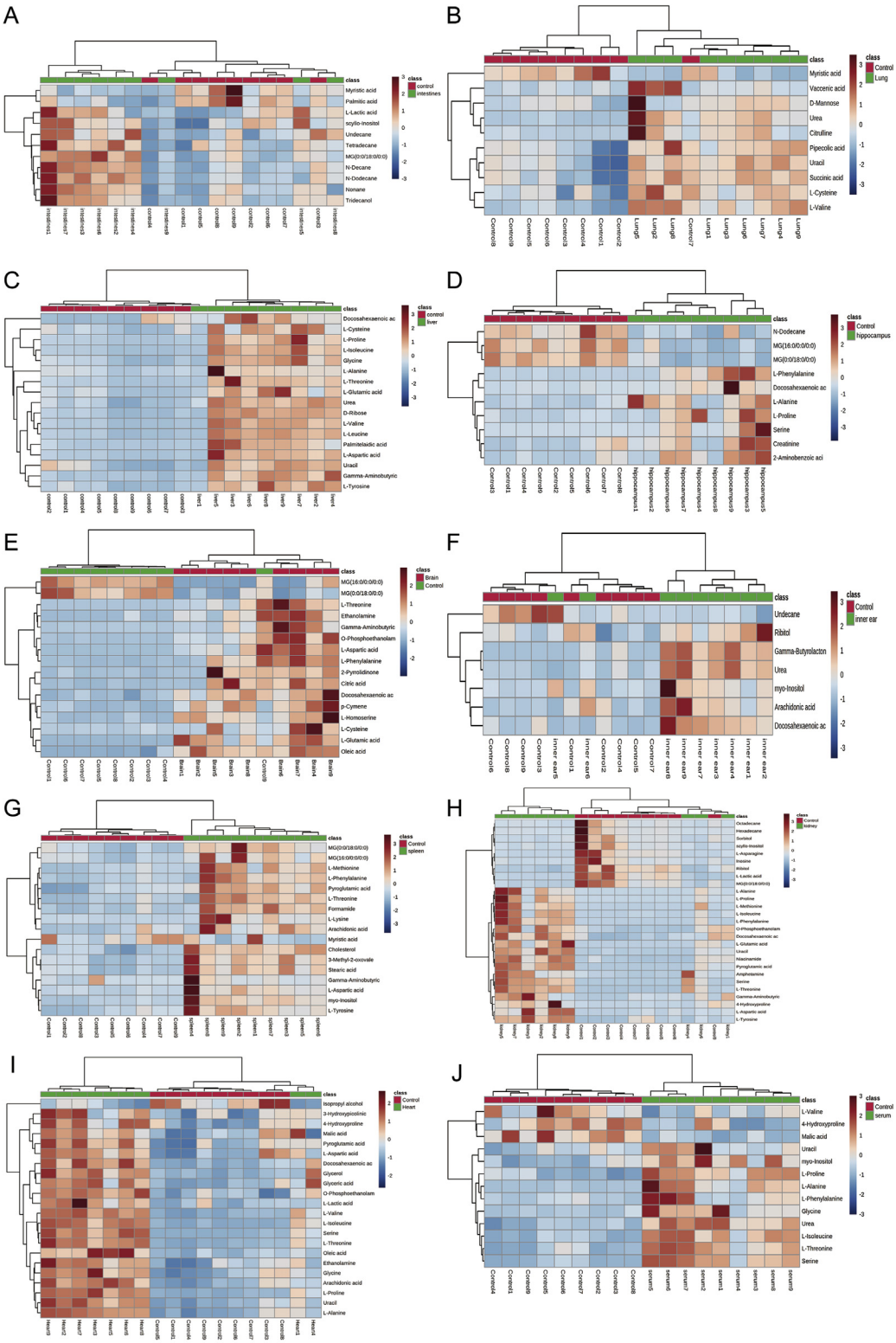

Figure 3. Heatmap of differential metabolites in (A) Intestine (B) Lung (C) Liver (D) Hippocampus (E) Cerebral cortex (F) Inner ear (G) Spleen (H) Kidney (I) Heart (J) Serum in the VCM group compared with controls. The color of each part represents the importance of metabolite changes (blue, down-regulated; red, up-regulated). Rows represent samples, and columns represent metabolites.

examined using HE staining. The results depicted that the boundary between renal cortex and renal medulla was obvious in the control group. The morphology of renal glomerulus and tubules were normal, with no cast formation, no obvious atrophy or necrosis, and regularly arranged luminal brush border in the tubular. No obvious abnormality was found in medulla. In addition, there was no obvious lymphocytes infiltration (Figure 6A-B). After VCM treatment, the pathological results showed extensive tubular atrophy (black arrow), renal tubular distension (red

Table 3. Pathway analysis performed using MetaboAnalyst 5.0 software.

Samples	Pathway Names	Raw p	Impact
Serum	Arginine and proline metabolism	0.04	0.14
	Glycine, serine and threonine Metabolism	0.03	0.30
	Phenylalanine, tyrosine and tryptophan biosynthesis	0.03	0.50
Liver	Alanine, aspartate and glutamate metabolism	0.00	0.51
	Arginine and proline metabolism	0.01	0.19
	Arginine biosynthesis	0.00	0.12
	Glutathione metabolism	0.00	0.11
	Glycine serine and threonine metabolism	0.00	0.30
	Butanoate metabolism	0.01	0.03
	Phenylalanine, tyrosine and tryptophan biosynthesis	0.04	0.50
	Glyoxylate and dicarboxylate metabolism	0.04	0.11
Kidney	Alanine, aspartate and glutamate metabolism	0.00	0.51
	Arginine and proline metabolism	0.00	0.25
	Arginine biosynthesis	0.02	0.12
	Butanoate metabolism	0.02	0.03
	Nicotinate and nicotinamide metabolism	0.02	0.19
	Phenylalanine metabolism	0.02	0.36
	Phenylalanine, tyrosine and tryptophan biosynthesis	0.00	1.00
Heart	Glycerolipid metabolism	0.02	0.33
	Glycine, serine and threonine metabolism	0.01	0.32
Cerebral cortex	Alanine, aspartate and glutamate metabolism	0.00	0.51
	Arginine and proline metabolism	0.03	0.11
	Arginine biosynthesis	0.01	0.12
	Butanoate metabolism	0.01	0.03
	Glutathione metabolism	0.02	0.02
	Glycerophospholipid metabolism	0.03	0.04
	Glycine, serine and threonine metabolism	0.03	0.02
	Glyoxylate and dicarboxylate metabolism	0.03	0.03
	Phenylalanine, tyrosine and tryptophan biosynthesis	0.03	0.50
Lung	Arginine biosynthesis	0.00	0.23
Spleen	Alanine, aspartate and glutamate metabolism	0.03	0.31
	Phenylalanine metabolism	0.01	0.36
	Phenylalanine, tyrosine and tryptophan biosynthesis	0.00	1.00
Intestine	Fatty acid biosynthesis	0.03	0.01
Hippocampus	Phenylalanine, tyrosine and tryptophan biosynthesis	0.02	0.50

Raw P value <0.05 and Impact >0 were considered to have significant differences in metabolic pathways.

arrow), protein accumulation within the tubules (blue arrow), along with obvious necrotic cell fragments (green arrow), and lymphocytes infiltration (yellow arrow) (Figure 6C-D).

4. Discussion

VCM is a glycopeptide antibacterial drug that has a significant bactericidal effect against gram-positive bacteria [18], MRSA [19], streptococci, enterococci, actinomycetes, clostridia, and eubacteria [20]. The usage of VCM can result in severe adverse effects, and among these incidental consequences, VCM has been reported to induce metabolic disorders including lipidomic alterations, disturbances of glucose metabolism and glutathione synthesis enhancement [15]. However, the systemic metabolic profiling after VCM treatment remain poorly elucidated. Therefore, in this study, a GC-MS approach was employed to investigate metabolic alterations in serum and several tissue samples (the intestine, lung, liver, hippocampus, cerebral cortex, inner ear, spleen, kidney, and heart) of VCM-treated mice. To the best of our knowledge, the current study represents the first comprehensive investigation of potential metabolic biomarkers of mice exposed to VCM, which may facilitate researchers to understand the pathogenesis of VCM-induced toxicity.

According to the results of pathway analysis, several amino acid pathways, such as alanine, aspartate and glutamate metabolism, arginine and proline metabolism, arginine biosynthesis, and phenylalanine, tyrosine and tryptophan biosynthesis were both disrupted in the kidney, liver, and cerebral cortex. In addition, disrupted butanoate metabolism was found in the kidney, liver, and cerebral cortex; glyoxylate and dicarboxylate metabolism was also found in the liver and cerebral cortex. Specially, nicotinate and nicotinamide metabolism alteration in the kidney, and glycerophospholipid metabolism in cerebral cortex were observed. Therefore, we speculated that the most affected organs by VCM were kidney, liver, and cerebral cortex. Blood-brain barrier is a functional barrier, which can exclude serum components from neuronal tissue, and maintain the homeostasis in the central nervous system. The ability of antibiotics to reach the infection compartment depends on their molecular weight, lipophilicity, the ability to bind to proteins, and the permeability of blood-brain barrier. It is well known that VCM is hydrophilic and it penetrate poorly through the blood-brain barrier. Therefore, in this study, VCM-induced metabolic changes in cerebral cortex may due the comprehensive metabolic alterations. The impacts of VCM on cerebral cortex metabolism need to be further investigated.

Amino acids, as important substrates, play a regulatory role in many metabolic pathways and function as diagnostic markers of many diseases [21]. Compared with the control group, amino acids including L-glutamic acid, valine, cystine, glycine, L-alanine, L-phenylalanine, L-tyrosine, threonine, L-proline, and L-aspartic acid were up-regulated in VCM group. Glutamate is a precursor of glutathione (GSH) [22], and GHS is a major endogenous antioxidant. VCM mice exhibited significantly increased L-glutamate levels in the liver, kidney, and cerebral cortex, which might be related to increased glutathione and glutathione disulfide bonds in parallel, indicating that a redox imbalance occurred [23]. Therefore, it was speculated that VCM administration induced a redox imbalance in the liver, kidney, and cerebral cortex. As amino acids are mainly metabolized in the liver [24], the dysregulations of alanine, aspartate and glutamate metabolism, arginine and proline metabolism, arginine biosynthesis, glycine serine and threonine metabolism, and phenylalanine, tyrosine and tryptophan biosynthesis may lead to liver injury in this study. In addition, liver dysfunction induced the urea synthesis disrupted, resulting in elevated urea in the liver and lung. It was suspected that alanine aspartate and glutamate metabolism, arginine and proline metabolism, arginine biosynthesis, and phenylalanine, tyrosine and tryptophan biosynthesis in the kidney and cerebral cortex were associated with VCM-induced toxicity. Overall, the changes in amino acid metabolism in the serum, liver, kidney, heart, cerebral cortex, spleen, and hippocampus of VCM mice may shed light on the pathogenesis of VCM-induced toxicity.

Nicotinic acid, also known as vitamin B3, generates the precursors of nicotinamide adenine dinucleotide (NAD^+) and NAD phosphate ($NADP^+$), and can be converted to nicotinamide, which is crucial for cellular electron transfer reactions and participate in energy metabolism [25]. Grison and colleagues conducted a multiscale high-throughput multi-omics approach to investigate the effect of low-dose uranium on rat kidneys; the results confirmed that nicotinate and disturbance of nicotinamide metabolism contributed to the low-dose uranium-induced nephrotoxicity [26]. A previous study demonstrated that cisplatin usage apparently disrupted energy generation through affecting nicotinate and nicotinamide metabolism in renal cells using HPLC-TOF/MS-based untargeted urine and kidney metabolomics in rats, which might be implicated in oxidative stress injury, inflammation, and renal cell membrane damage; however, cisplatin significantly down-regulated

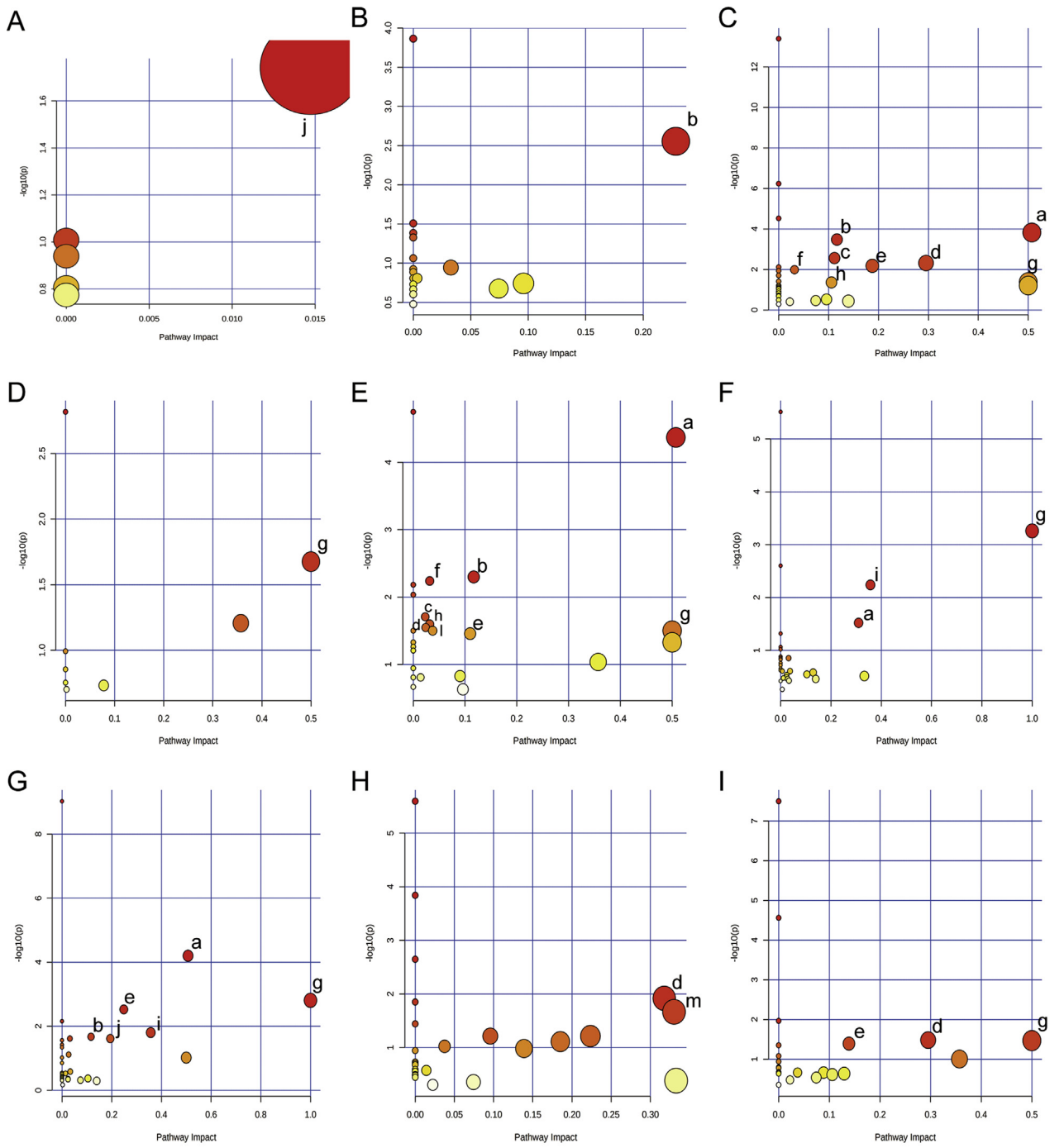

Figure 4. Summary of pathway analysis performed using MetaboAnalyst 5.0. (A) Intestine: (j) Fatty acid biosynthesis. (B) Lung: (b) Arginine biosynthesis. (C) Liver: (a) Alanine aspartate and glutamate metabolism; (b) Arginine biosynthesis; (c) Glutathione metabolism; (d) Glycine serine and threonine metabolism; (e) Arginine and proline metabolism; (f) Butanoate metabolism; (g) Phenylalanine tyrosine and tryptophan biosynthesis; (h) Glyoxylate and dicarboxylate metabolism. (D) Hippocampus: (g) Phenylalanine tyrosine and tryptophan biosynthesis. (E) Cerebral cortex: (a) Alanine aspartate and glutamate metabolism; (b) Arginine biosynthesis; (c) Glutathione metabolism; (d) Glycine serine and threonine metabolism; (e) Arginine and proline metabolism; (f) Butanoate metabolism; (g) Phenylalanine tyrosine and tryptophan biosynthesis; (h) Glyoxylate and dicarboxylate metabolism; (l) Glycerophospholipid metabolism; (F) Spleen: (a) Alanine aspartate and glutamate metabolism; (i) Phenylalanine metabolism; (g) Phenylalanine tyrosine and tryptophan biosynthesis; (G) Kidney: (a) Alanine aspartate and glutamate metabolism; (b) Arginine Biosynthesis; (e) Arginine and proline metabolism; (f) Butanoate metabolism; (g) Phenylalanine tyrosine and tryptophan biosynthesis; (i) Phenylalanine metabolism; (j) Nicotinate and nicotinamide metabolism; (H) Heart: (d) Glycine serine and threonine metabolism; (m) Glycerolipid metabolism; (I) Serum: (d) Glycine serine and threonine metabolism; (e) Arginine and proline metabolism; (g) Phenylalanine tyrosine and tryptophan biosynthesis.

nicotinamide level [27], which was inconsistent with our results. In this study, the results showed that the level of nicotinamide was up-regulated in VCM group. Therefore, the discrepancy between the above study and our study needs further investigation. In addition, it has been reported that the nicotinate and nicotinamide metabolism may be involved in the inflammatory response, and it is associated with some metabolic enzymes and secondary metabolites produced during the metabolic processes [28]. In the present study, the level of nicotinamide was increased

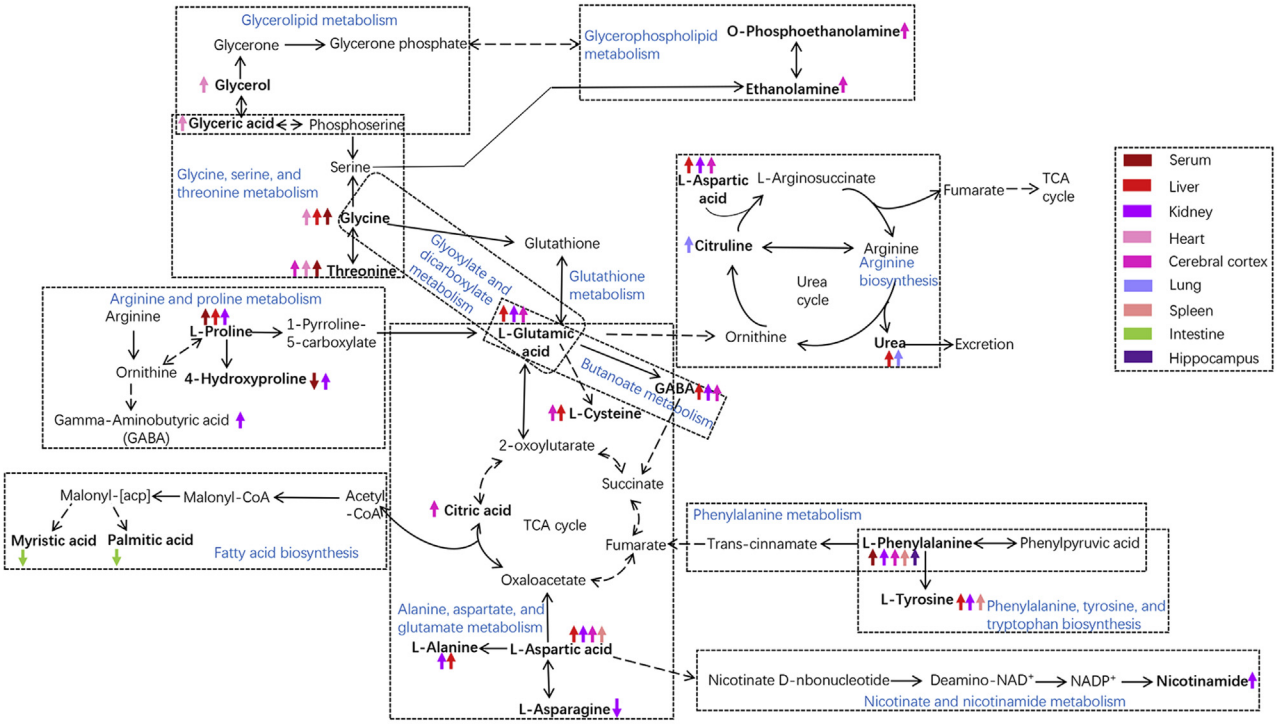

Figure 5. Schematic diagram of related metabolic pathways affected by VCM in serum and major tissues. Disrupted metabolic pathways were marked in blue. Solid arrows represent a single process, while dashed arrows represent multiple processes. Differential metabolites enriched in pathways were marked in bold. The upward arrows represent the up-regulated metabolites, while the downward arrows represent the down-regulated metabolites.

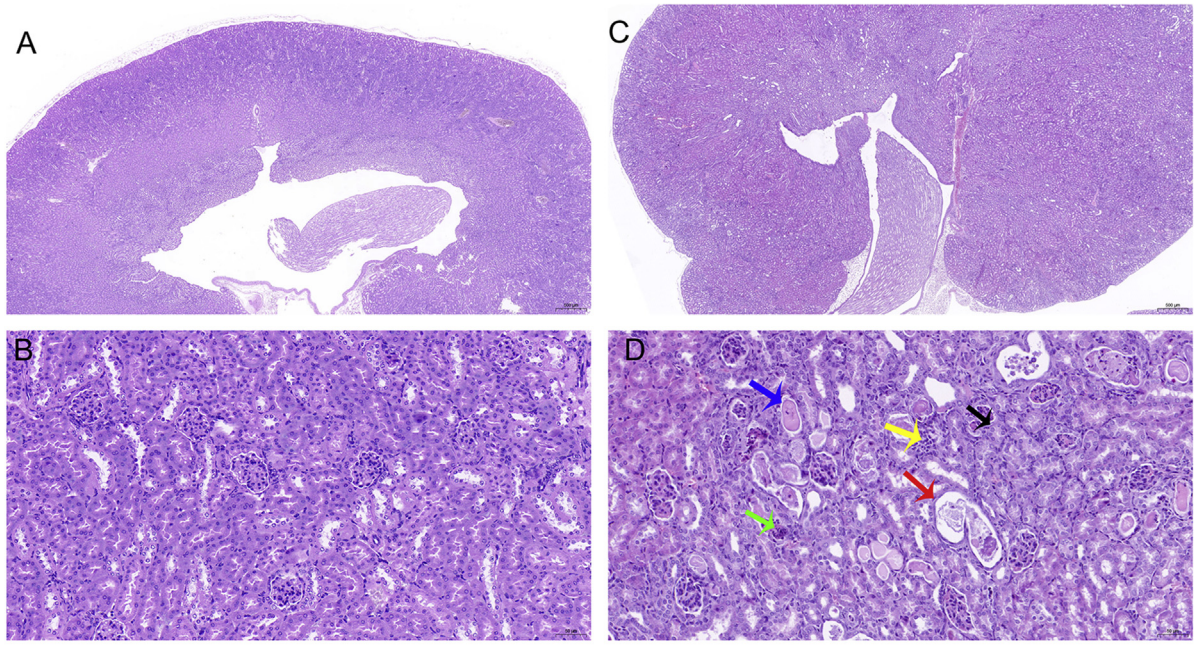

Figure 6. Pathological examination of kidney tissue was examined using HE staining. A-B, Pathological examination of kidney tissue in control group (A, magnification 2.0x; B, magnification 20.0x). C-D, Pathological changes of kidney tissue in VCM group (C, magnification 2.0x; D, magnification 20.0x). Black arrow, renal tubular atrophy. Red arrow, renal tubular distension. Blue arrow, protein accumulation within the tubules. Green arrow, necrotic cell fragments. Yellow arrow, lymphocytes infiltration.

in VCM group, indicating that VCM induced nephrotoxicity mainly through regulating the nicotinate and nicotinamide metabolism-related energy metabolism and inflammatory response.

Glutamic acid is a substrate in the bioproduction of gamma-aminobutyric acid (GABA), which is one of the important inhibitory neurotransmitters in mammal central nervous system. As an intermediary metabolite, 2-oxoglutarate connects with glutaminolysis in the TCA cycle wherein the glutamic acid derived from 2-oxoglutarate transforms to GABA [29]. Besides, with the presence of GABA aminotransferase, GABA can convert to succinate semialdehyde, and then the succinate

finally enters the TCA cycle in the energy metabolism process. In this study, the aberrant citric acid indicated the dysfunction of TCA cycle, which might be induced by the disrupted butanoate metabolism wherein L-glutamic acid and GABA were up-regulated in the kidney, cerebral cortex, and liver. Additionally, the glyoxylate and dicarboxylate metabolism pathway contributes to the TCA cycle in the energy metabolism process [30]. This study identified that the glyoxylate and dicarboxylate metabolism pathway was disrupted in the kidney, cerebral cortex, and liver, suggesting that disrupted L-glutamic acid and glyoxylate and dicarboxylate metabolism was implicated in the dysfunction of TCA cycle, leading to energy metabolism dysfunction. Moreover, a compelling evidence identified that the GABA metabolism and synthesis exerted a regulatory effect on the stress response of cancer cells [31]. In unsaturated fatty acids and the butanoate metabolism pathways, the disruptions of docosahexaenoic acid, arachidonic acid, L-glutamic glutamate, and succinic acid contributed to inflammatory responses and dysfunctional immune function in patients with chronic spontaneous urticaria [32]. Collectively, in the present study, the findings suggested that dysregulated butanoate metabolism, and glyoxylate and dicarboxylate metabolism in energy metabolism and inflammatory responses might be responsible for VCM-induced toxicity in the kidney, cerebral cortex, and liver. This study represents the first discovery of butanoate metabolism disruption in kidney, cerebral cortex, and liver after VCM application.

In patients with heart failure, lipid metabolism pathways, such as sphingolipid metabolism and glycerolipid metabolism have been discovered using metabolomic and lipidomic analyses [33]. In addition, the glycerophospholipid metabolism was associated with lipopolysaccharide-induced multiple organ injury, and the glycerophospholipid metabolism was involved in macrophage-driven inflammatory response [34]. It has been reported that neural membrane glycerophospholipids and polyunsaturated fatty acids are precursors for lipid mediators, which regulate neuroinflammation, neural cell proliferation, differentiation, and apoptosis [35]. Thus, it is implied that the glycerolipid metabolism and glycerophospholipid metabolism play crucial roles in inflammatory responses. In this study, the levels of glycerol and glyceric acid were patently up-regulated in the heart, indicating that the glycerolipid metabolism was dramatically disturbed after VCM application. Meanwhile, the glycerophospholipid metabolism was also disrupted in the cerebral cortex, indicating that glycerophospholipid metabolism might contribute to neuroinflammation in the cerebral cortex. The results suggested that VCM administration-induced toxicity might be associated with the glycerolipid metabolism and glycerophospholipid metabolism-provoked inflammatory responses in the heart and cerebral cortex.

Fatty acid intake plays a crucial role in regulation of gut microbiota composition, and their interaction with hosts is related to metabolic dysbiosis or other diseases [36]. Among diverse fatty acid, myristic acid and palmitic acid are the main saturated fatty acids. It is supported that palmitic acid, specifically in sn-2 configuration, imparts benefits for intestinal mucosal homeostasis, gut microbiome, and immune response to avoiding intestinal injury [37]. Ding demonstrated that palmitic acid-altered intestinal microbiota could indirectly lead to endoplasmic reticulum stress, and consequently, liver damage occurred in zebrafish; moreover, palmitic acid-altered microbiota enhanced the absorption of palmitic acid and its overflow to the liver, which induced endoplasmic reticulum stress and exacerbated the hepatotoxicity [38]. Additionally, Prasath and colleagues confirmed that co-administration of myristic acid and palmitic acid exerted a synergistic anti-inflammatory effect on systemic candidiasis and candidemia [39]. Similarly, myristic acid and palmitic acid-enriched *nigella sativa* could alleviate cisplatin-induced nephrotoxicity in rats [40]. In the current study, administration of VCM-induced significant down-regulation of intestinal myristic acid and palmitic acid, indicating that VCM might alter the intestinal microbiota that resulted in their absorption or overflow. Besides, it is speculated that myristic acid and palmitic acid-altered microbiome metabolism may contribute to VCM-induced immune response or pro-inflammatory response.

This study typically focused on the alterations of metabolic profiling in mice, whilst there is lacking of further validation. Thus, clinical samples should be collected from patients who received VCM treatment, and metabonomic analysis should be conducted to validate our study. Only a single analytical approach was employed in this research, therefore, the metabolic changes in VCM-treated mice need further verification using multi-omics approaches.

In conclusion, the present study used GC-MS to comprehensively investigates the metabolic profiling of tissues and various organs in mice after VCM exposure. We found that VCM affects amino acid metabolism, energy metabolism, fatty acid biosynthesis and lipid metabolism. The data provide comprehensive insights into metabolomic identification after VCM administration.

Declarations

Author contribution statement

Changmeng Cui: Performed the experiments; Wrote the paper.
Li Zhu: Performed the experiments; Wrote the paper.
Qian Wang, Ruijuan Liu, Dadi Xie: Analyzed and interpreted the data.
Yujin Guob, Pei Jiang: Conceived and designed the experiments.
Dingyi Yu, Changshui Wanga, Dan Chen: Contributed reagents, materials, analysis tools or data.

Funding statement

This work was supported by Bethune Charitable Foundation [B-19-H-20200622].
This work was supported by Scientific Research Foundation of Shandong Medical Association [YXH2020ZX053].
This work was supported by Natural Science Foundation of Shandong Province [ZR2020MH375].
This work was supported by Taishan Scholar Project of Shandong Province [tsqn201812159].

Data availability statement

Data will be made available on request.

Declaration of interests statement

The authors declare no conflict of interest.

Additional information

No additional information is available for this paper.

Acknowledgements

Not applicable.

References

[1] A.H. Kim, Y. Lee, E. Kim, et al., Assessment of oral vancomycin-induced alterations in gut bacterial microbiota and metabolome of healthy men, Front. Cell. Infect. Microbiol. (2021) 11.
[2] K. Doerries, R. Schlueter, M. Lalk, Impact of antibiotics with various target sites on the metabolome of Staphylococcus aureus, Antimicrob. Agents Chemother. 58 (2014) 7151–7163.
[3] M.J. Rybak, J. Le, T.P. Lodise, et al., Validity of 2020 vancomycin consensus recommendations and further guidance for practical application, Am. J. Health Syst. Pharm. 78 (2021) 1364–1367.
[4] R.G. Smith, Vancomycin - an overview for the podiatric physician, J. Am. Podiatr. Med. Assoc. 94 (2004) 389–394.
[5] C.P. Rosa, J.A. Pereira, N. Cristina de Melo Santos, et al., Vancomycin-induced gut dysbiosis during Pseudomonas aeruginosa pulmonary infection in a mice model, J. Leukoc. Biol. 107 (2020) 95–104.

[6] A. Vrieze, C. Out, S. Fuentes, et al., Impact of oral vancomycin on gut microbiota, bile acid metabolism, and insulin sensitivity, J. Hepatol. 60 (2014) 824–831.
[7] H. Du, Z. Li, Y. Yang, et al., New insights into the vancomycin-induced nephrotoxicity using in vitro metabolomics combined with physiologically based pharmacokinetic modeling, J. Appl. Toxicol. 40 (2020) 897–907.
[8] N. Gupta, S. Vats, P. Bhargava, Sustainable agriculture: role of metagenomics and metabolomics in exploring the soil microbiota, in: Silico Approach for Sustainable Agriculture, Springer, 2018, pp. 183–199.
[9] M. Shoaib, R.C. Choudhary, J. Choi, et al., Plasma metabolomics supports the use of long-duration cardiac arrest rodent model to study human disease by demonstrating similar metabolic alterations, Sci. Rep. 10 (2020) 1–14.
[10] H. Pang, W. Jia, Z. Hu, Emerging applications of metabolomics in clinical pharmacology, Clin. Pharmacol. Ther. 106 (2019) 544–556.
[11] W. Xing, L. Gu, X. Zhang, et al., A metabolic profiling analysis of the nephrotoxicity of acyclovir in rats using ultra performance liquid chromatography/mass spectrometry, Environ. Toxicol. Pharmacol. 46 (2016) 234–240.
[12] J. Hummel, S. Segu, Y. Li, et al., Ultra performance liquid chromatography and high resolution mass spectrometry for the analysis of plant lipids, Front. Plant Sci. 2 (2011).
[13] S. Ekins, Y. Nikolsky, T. Nikolskaya, Techniques: application of systems biology to absorption, distribution, metabolism, excretion and toxicity, Trends Pharmacol. Sci. 26 (2005) 202–209.
[14] C. Geng, Y. Guo, C. Wang, et al., Comprehensive evaluation of lipopolysaccharide-induced changes in rats based on metabolomics, J. Inflamm. Res. 13 (2020) 477–486.
[15] S. Lagies, R. Pichler, G. Vladimirov, et al., Metabolic and lipidomic assessment of kidney cells exposed to nephrotoxic vancomycin dosages, Int. J. Mol. Sci. 22 (2021), 10111.
[16] A.H. Kim, Y. Lee, E. Kim, et al., Assessment of oral vancomycin-induced alterations in gut bacterial microbiota and metabolome of healthy men, Front. Cell. Infect. Microbiol. 11 (2021) 412.
[17] M.R. Viant, I.J. Kurland, M.R. Jones, et al., How close are we to complete annotation of metabolomes? Curr. Opin. Chem. Biol. 36 (2017) 64–69.
[18] F.R. Bruniera, F.M. Ferreira, L.R.M. Saviolli, et al., The use of vancomycin with its therapeutic and adverse effects: a review, Eur. Rev. Med. Pharmacol. Sci. 19 (2015) 694–700.
[19] A. Weston, H.W. Boucher, Early high-dose daptomycin for methicillin-resistant Staphylococcus aureus bloodstream infections with elevated vancomycin minimum inhibitory concentrations: ready for prime time? Clin. Infect. Dis. 56 (2013) 1570–1572.
[20] M.D. Nailor, J.D. Sobel, Antibiotics for gram-positive bacterial infections: vancomycin, teicoplanin, quinupristin/dalfopristin, oxazolidinones, daptomycin, dalbavancin, and telavancin, Infect. Dis. Clin. 23 (2009) 965. -+.
[21] M.A. Razak, P.S. Begum, B. Viswanath, et al., Multifarious beneficial effect of nonessential amino acid, Glycine: a review, Oxid. Med. Cell. Longev. 2017 (2017).
[22] J.P. Mothet, L. Pollegioni, G. Ouanounou, et al., Glutamate receptor activation triggers a calcium-dependent and SNARE protein-dependent release of the gliotransmitter D-serine, Proc. Natl. Acad. Sci. U. S. A 102 (2005) 5606–5611.
[23] I. Hirahara, E. Kusano, D. Jin, et al., Hypermetabolism of glutathione, glutamate and ornithine via redox imbalance in methylglyoxal-induced peritoneal injury rats, J. Biochem. 167 (2020) 185–194.
[24] I. Campbell, Liver: metabolic functions, Anaesth. Intensive Care Med. 7 (2006) 51–54.
[25] M. Fontecha-Barriuso, A.M. Lopez-Diaz, S. Carriazo, et al., Nicotinamide and Acute Kidney Injury, Oxford University Press, 2021, pp. 2453–2462.
[26] S. Grison, D. Kereselidze, D. Cohen, et al., Applying a multiscale systems biology approach to study the effect of chronic low-dose exposure to uranium in rat kidneys, Int. J. Radiat. Biol. 95 (2019) 737–752.
[27] X. Qu, H. Gao, J. Sun, et al., Identification of key metabolites during cisplatin-induced acute kidney injury using an HPLC-TOF/MS-based non-targeted urine and kidney metabolomics approach in rats, Toxicology 431 (2020) 152366.
[28] L. Gong, L. Yu, X. Gong, et al., Exploration of anti-inflammatory mechanism of forsythiaside A and forsythiaside B in CuSO4-induced inflammation in zebrafish by metabolomic and proteomic analyses, J. Neuroinflammation 17 (2020) 1–21.
[29] L.L. Mamuad, S.-S. Lee, The role of glutamic acid-producing microorganisms in rumen microbial ecosystems, J. Life Sci. 31 (2021) 520–526.
[30] Y. Song, T. Hu, H. Gao, et al., Altered metabolic profiles and biomarkers associated with astragaloside IV-mediated protection against cisplatin-induced acute kidney injury in rats: an HPLC-TOF/MS-based untargeted metabolomics study, Biochem. Pharmacol. 183 (2021) 114299.
[31] J.E. Ippolito, D. Piwnica-Worms, A fluorescence-coupled assay for gamma aminobutyric acid (GABA) reveals metabolic stress-induced modulation of GABA content in neuroendocrine cancer, PLoS One 9 (2014) e88667.
[32] D. Wang, S. Guo, H. He, et al., Gut microbiome and serum metabolome analyses identify unsaturated fatty acids and butanoate metabolism induced by gut microbiota in patients with chronic spontaneous urticaria, Front. Cell. Infect. Microbiol. 10 (2020) 24.
[33] D. Contaifer Jr., L.F. Buckley, G. Wohlford, et al., Metabolic modulation predicts heart failure tests performance, PLoS One 14 (2019) e0218153.
[34] S. Wang, K.S. Tan, H. Beng, et al., Protective effect of isosteviol sodium against LPS-induced multiple organ injury by regulating of glycerophospholipid metabolism and reducing macrophage-driven inflammation, Pharmacol. Res. 172 (2021) 105781.
[35] A.A. Farooqui, L.A. Horrocks, T. Farooqui, Modulation of inflammation in brain: a matter of fat, J. Neurochem. 101 (2007) 577–599.
[36] D.J. Machate, P.S. Figueiredo, G. Marcelino, et al., Fatty acid diets: regulation of gut microbiota composition and obesity and its related metabolic dysbiosis, Int. J. Mol. Sci. 21 (2020) 4093.
[37] D. Ramiro-Cortijo, P. Singh, Y. Liu, et al., Breast milk lipids and fatty acids in regulating neonatal intestinal development and protecting against intestinal injury, Nutrients 12 (2020) 534.
[38] Q. Ding, Z. Zhang, C. Ran, et al., The hepatotoxicity of palmitic acid in zebrafish involves the intestinal microbiota, J. Nutr. 148 (2018) 1217–1228.
[39] K.G. Prasath, R. Alexpandi, R. Parasuraman, et al., Anti-inflammatory potential of myristic acid and palmitic acid synergism against systemic candidiasis in Danio rerio (Zebrafish), Biomed. Pharmacother. 133 (2021) 111043.
[40] A.M. Alsuhaibani, Effect of Nigella sativa against cisplatin induced nephrotoxicity in rats, Ital. J. Food Saf. 7 (2018).